ISSN 2070-2051, Protection of Metals and Physical Chemistry of Surfaces, 2011, Vol. 47, No. 5, pp. 645–653. © Pleiades Publishing, Ltd., 2011.

NEW SUBSTANCES, MATERIALS, AND COATINGS

Optimization of Deposition Conditions for Bright Zn–Fe Coatings and its Characterization[1]

Ramesh Bhat[a], Udaya Bhat K[b], and A. Chitharanjan Hegde[a]

[a] *Electrochemistry Research Laboratory, Department of Chemistry*

[b] *Department of Metallurgy and Materials Engineering National Institute of Technology Karnataka, Surathkal Srinivasnagar–575 025, India*

e-mail: achegde@rediffmail.com

Received August 4, 2010

Abstract—Sulfate bath having $ZnSO_4 \cdot 7H_2O$, $Fe_2(SO_4)_3 \cdot H_2O$ and thiamine hydrochloride (THC) and citric acid (CA) in combination, represented as (THC + CA) was optimized for deposition of bright Zn-Fe alloy coating on mild steel. Bath constituents and operating parameters were optimized by standard Hull cell method, for peak performance of the coating against corrosion. The effect of current density (c.d.), pH and temperature on deposit characters, such as corrosion resistance, hardness and glossiness were studied and discussed. Potentiodynamic polarization and electrochemical impedance spectroscopy (EIS) methods were used to assess the corrosion behaviors. Surface morphology, and composition of the coatings were examined using Scanning Electron Microscopy (SEM), interfaced with EDXA facility, respectively. The Zn–Fe alloy, with intense peaks corresponding to Zn(100) and Zn(101) phases, showed highest corrosion resistance, evidenced by X-ray diffraction (XRD) study. A new and cheap sulfate bath, for bright Zn–Fe alloy coating on mild steel has been proposed, and results are discussed.

DOI: 10.1134/S2070205111050030

1. INTRODUCTION

Zn alloy electroplating appears to be one of the most earliest and easiest method for getting high protection against corrosion [1] and commonly used metals for alloying are of Fe group [2–4]. Among Zn–M (where M = Ni, Co, Fe and less commonly Mn) alloys, Zn–Fe alloys is less used in industry as protective coatings on account of their less corrosion resistance [5]. The electrodeposition of Zn–Fe alloys is generally classified as anomalous codeposition process due to the preferential deposition of the less noble metal, Zn [1]. Several hypotheses have been proposed to explain this anomalous codeposition. The most accepted hypothesis explains the anomalous behavior in terms of the precipitation and adsorption of a zinc hydroxide film at the electrode surface that induces zinc reduction [6]. This zinc hydroxide film is formed due to the increase in interfacial pH during the simultaneous electrochemical reaction of hydrogen evolution. An alternative hypothesis, was discussed by [7], suggests that the under potential deposition (UPD) of Zn inhibits the deposition of Fe.

The electrodeposition of Zn–Fe alloys from a chloride-based electrolyte has been studied using electrochemical polarization techniques and other instrumental methods [8]. Zn–Fe alloys with compositions ranging from 5 wt % to more than 75 wt % Fe have been electrodeposited from a single bath, showing this system ideal for production of composition modulated alloy (CMA) electrodeposits. The study on the behavior of Zn, Fe and Zn–Fe alloy onto copper from acid chloride solutions containing, EDTA– 2Na and boric acid was investigated by means of cyclic voltammetry and the steady state polarization technique [9]. It was found that deposition of Zn–Fe followed the mechanism of three dimensional nucleation and subsequent grain growth. The Zn^{+2} ions in the electrolyte inhibit the deposition of Fe, while Fe^{+2} ions promote the deposition of Zn. It was found that the codeposition of Zn and Fe behaved anomalously. A sulfate bath was developed for the preparation of Zn–Fe alloy coatings by [10]. Citric acid and sodium citrate were used as buffer and complexing agents, respectively. The wt % Fe in the deposit was found to be The wt % Fe in the deposit found to increase with current density. The kinetics of Zn–Fe codeposition was investigated in acid solutions [11]. The effects of solution composition and pH were analyzed. Inhibition of H^+ reduction and Fe deposition occurs with increasing Zn^{+2} ions in sulfate solution. It was found that the kinetics of metal deposition is governed by the interfacial pH.

Thus many extensive research works have been reported on deposition mechanism of Zn–Fe group metal alloys, concentrating on anomalous codeposition; and dependency of deposit characters, with bath constitutions and operating parameters. But no work is reported in relation to optimization of Zn–Fe alloy bath, using Thiamine hydrochloride (THC) in con-

[1] The article is published in the original.

junction with citric acid (CA), for bright Zn–Fe alloy coatings. In the present study, the role of THC and CA in combination, on electrodeposition of Zn–Fe alloy and its corrosion protection performance are investigated. The focus of this work is to optimize the bath compositions and operating parameters, and characterize the coatings. Cyclic voltammetry was used to study the mechanism of codeposition with/without additives. Techniques such as scanning electron microscopy (SEM), Energy Dispersive X–ray Analysis (EDXA) and X–ray diffraction (XRD) methods were used to characterize the coatings.

2. EXPERIMENTAL PROCEDURE

Plating solutions were prepared from reagent grade chemicals and distilled water. Standard Hull cell, of 267 ml capacity was used to optimize bath constituents. All depositions were carried out at 303K and pH 4.0, except during their variation. Polished mild steel panels were used as cathode (area 7.5 cm^2) and pure zinc plate, with same exposed surface area was used as anode. A PVC cell, of 250 cm^3 in capacity was used with cathode-anode space of ~5 cm. All depositions were carried out galvanostatically under common conditions of temperature and pH for duration of 10 minutes (for comparison purpose), using sensitive power source (N6705A, Agilest Technologies). Thiamine hydrochloride (THC) and citric acid (CA) in combination, represented as (THC +CA) was used as additive for improving the brightness and homogeneity of the deposit. The constituents and deposition parameters were optimized, based on the appearance and corrosion resistance of the coatings.

In order to evaluate the electrochemical properties of the coatings, potentiodynamic polarization and electrochemical impedance spectroscopy (EIS) measurements were performed. All electrochemical tests were carried out using Potentiostat/Galvanostat (VersaSTAT–3, Princeton Applied Research) using a three-electrode cell. The working electrode was coated metal specimen. The counter electrode was a platinum electrode, with same surface area as working electrode. All electrochemical potentials referred in this work are indicated relative to saturated silver/silver chloride electrode ($Ag/AgCl/Cl^-_{sat.}$). The 5% NaCl solution was used as corrosion medium throughout the study. Potentiodynamic polarization study was carried out in a potential ramp of –0.25 V to +0.25V around open circuit potential (OCP), at scan rate of 1 mVs^{-1}. Corrosion rates were determined by Tafel's extrapolation method. The impedance measurements were carried out over frequency range of 100 kHz to 20 mHz, using sine waves of 10 mV amplitude. Role of Additives was investigated by studying the cyclic polarization in a potential range of –1.4 V to 0.5 V.

The microstructure of the deposits were examined using SEM (JSM–6380 LA from JEOL, Japan). X–ray diffraction (XRD) patterns were collected on an JDX–8P JEOL, Japan, with CuKα radiation (k = 1.5418 Å) as the X–ray source. While the thickness of the deposits were calculated from Faradays law, it was verified using Digital Thickness Tester (Coatmeasure M&C, ISO–17025). The wt % Fe in the deposit was estimated by colorimetric method [12]. The hardness of the deposits (~20 μm thickness) was measured by Vickers method, using Micro Hardness Tester (CLEMEX). The cathode current efficiency (CCE) of the deposition was determined by knowing the mass and composition of the deposit [1]. The brightness and adhesion of deposit was measured using Gloss Meter (Nova–Elite, 60°) and cross cut Adhesion Tester (TQC—ASTM), respectively.

3. RESULTS AND DISCUSSIONS

3.1. Cyclic Voltammetry Study

The electrochemical behavior of the Zn–Fe alloys was studied from a base solution with and without (THC + CA). The preliminary experiments showed that (THC + CA) has no electrochemical activity, under the experimental conditions used in this study. The potential scan was started in the cathodic direction from the rest potential in the potential range 0.5 to –1.50 V vs. $Ag/AgCl/Cl^-_{sat.}$. Fig. 1 shows typical voltammograms obtained from solutions with and without additives. In the absence of (THC + CA), no reduction peak was observed. When the scan is reversed, three oxidation peaks are observed. The detection of multiple peaks during the electrochemical oxidation of alloys can be attributed to the dissolution of the metals in the alloy via different intermediate phases [13]. Introduction of (THC + CA) caused an important change in the voltammograms. During the cathodic scan, reduction peak is observed at more cathodic potential (–0.92V), against no peak observed in the absence of (THC + CA). This shift can be attributed to the effect of the adsorption of (THC + CA), which induces an overpotential in the alloy deposition process. During the anodic potential scan, a small anodic current density is observed in the range of –0.95 to –0.45 V vs $Ag/AgCl/Cl^-_{sat.}$, and two peaks appear, one at more cathodic potentials in the range –0.90 to –0.55V vs $Ag/AgCl/Cl^-_{sat.}$, and another small peak, at range of –0.40 to –0.30V vs. $Ag/AgCl/Cl^-_{sat.}$ (shown in inset), corresponding dissolution of alloy of another phase. Thus, the voltammetric response gives information regarding the characteristics of the components of the alloy, and the structure of the deposited phases. An important feature of the results presented above is that the addition of (THC + CA) inhibits the preferential deposition of zinc to form Zn–Fe alloy, with different phase structure, and favors the normal codeposition of the Zn–Fe alloy.

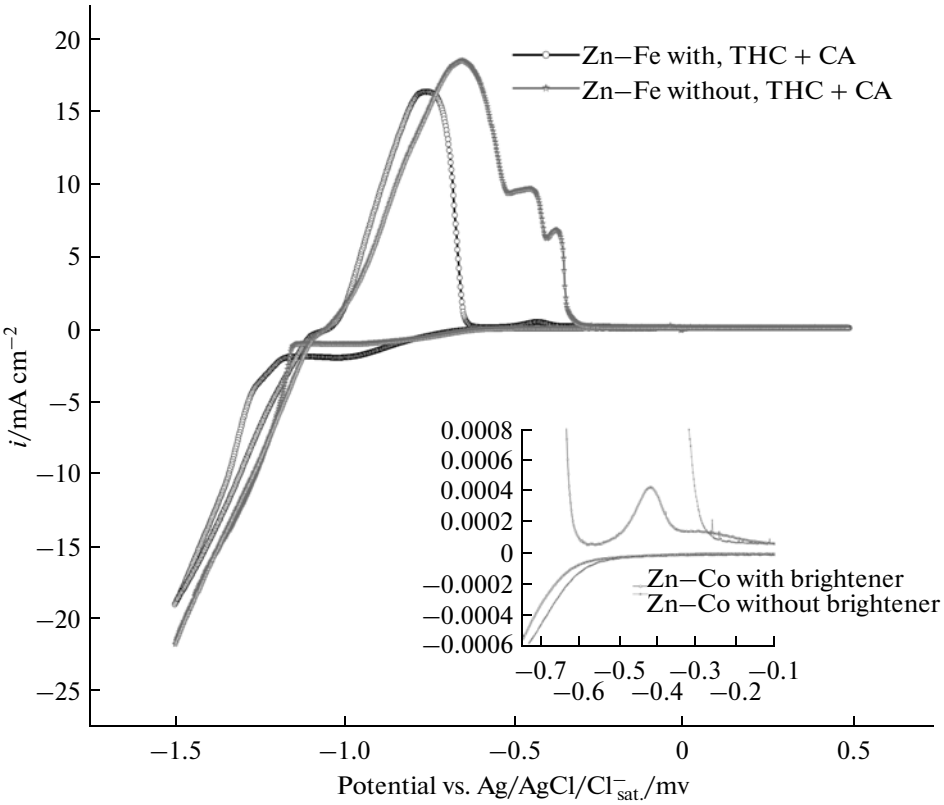

Fig. 1. Cyclic voltammograms for Zn–Fe bath, demonstrating the effects of (THC +CA). Working electrode: Pt, pH 4.0, T = 303K, v = 10 mV s^{-1}.

3.2. Hull Cell Study

Acid bath containing $ZnSO_4 \cdot 7H_2O$, $Fe_2(SO_4)_3 \cdot H_2O$ was optimized by conventional Hull cell method [14]. Addition of small amount (0.5 g/L) of thiamine hydrochloride (THC) was found to show substantial influence on the brightness of deposit. The citric acid (CA) was used as a buffer, to suppress the hydroxide formation. Deposits having grayish white/bright/porous appearance were obtained over wide c.d., 1.0–5.0 A/dm^2. Sodium acetate was used as conducting salt for improving the homogeneity of the deposit. Effect of each constituents was examined in terms of their influence on appearance, brightness and morphology of the coatings. Bath constituents and operating parameters arrived after optimization is shown in Table 1.

3.3. Effect of Current Density

The current density was found to be the key component on deposit characters, and are discussed as below.

I) Wt % Fe in the deposit

The change in appearance of the coatings, and wt % Fe in the deposit over range of c.d., 1.0–5.0 A/dm^2 is shown in Table 2. The bath produced grayish bright deposit towards low c.d. (~2.12 wt % Fe), and porous bright (~6.86 wt % Fe) deposit towards high c.d. A bright deposit was found at 3.0 A/dm^2 (~3.62 wt % Fe). Increase in wt % Fe with c.d. is attributed to the rapid depletion of more readily depositable (mrd) Zn^{+2} ions at cathode film [1]. The cathode current efficiency (CCE) of the bath was found to decrease

Table 1. Composition and operating parameters of optimized bath for electrodeposition of bright Zn–Fe alloy on to mild steel

Bath composition	Amount, g/L	Operating parameters
Zinc sulfate	70	pH : 4.0
Ferric sulfate	20	Temperature : 303K
Sodium acetate	60	Anode : Pure zinc
Thiamine hydrochloride	0.5	current density : 3.0 A/dm^2
Citric acid	4.0	

Table 2. Effect of current density on pH, wt % Fe, CCE, hardness, and glossiness and nature of Zn–Fe electroplates from optimized bath at 303 K

Current density, A/dm^2	pH of bath	wt % bath	CCE	Vickers hardness V_{200}	Glossiness unit	Appearance of the deposit
1.0	4.0	2.12	90.6	143	119.0	Grayish white
2.0	4.0	2.71	91.2	167	126.0	Bright
3.0	4.0	3.62	92.6	179	141.9	Bright
4.0	4.0	4.93	89.0	193	148.2	Bright
5.0	4.0	6.86	87.0	197	153.3	Porous bright
3.0	3.0	1.66	89.7	–	–	Grayish white
3.0	4.0	3.62	92.6	–	–	Bright
3.0	5.0	4.10	86.0	–	–	Porous bright

with c.d. as shown in Table 2, may be due to excessive evolution of hydrogen, during plating.

II) Hardness, Glossiness, and Adhesion Tests

Hardness of Zn–Fe alloy coatings was found to be increase with Fe content, as shown in Table 2. This may be ascribed by the high density of Fe, compared to Zn (d_{Zn}= 7.14 g cm^{-3} and d_{Fe} = 7.90 g cm^{-3}). The glossiness of the deposit was found to increase progressively with wt % Fe as shown in Table 2. However, thickness of the deposits was found to be increase substantially with c.d., may be due to intrusion metal hydroxide. Adhesion test showed that the coatings are hard adherent with completely smooth cut edges, and none of squares of the lattice is detached from the substrate.

III) Effect of pH

The effect of pH on deposit characters are shown in Table 2. At low pH, the deposit was found to be grayish white, whereas at high pH it was porous bright. The iron content of the alloy was found to increase with pH. Considerable increase in wt % Fe with pH indicated that the metal ions are in complex form due to additives [1].

Table 3. Effect of temperature on wt % Fe in the deposit at 3.0 A/dm^2 from bath having optimal compositions

Temp, K	wt % Fe in the deposit	Appearance of the deposit
283	6.2	Grayish
293	4.1	Bright
303	3.6	Bright
313	2.7	Bright
323	1.4	Porous bright

3.4. Effect of Temperature

Temperature also found to play a prominent role on composition and appearance of the deposit, as is the case in other Zn–M alloys. The deposit was found to be grayish (due to high wt % Fe) at low temperature, and silver bright (due to low wt % Fe) at high temperature, shown in Table 3. It may be noted that, at elevated temperature more readily depositable metal ions are favored to be replenished rapidly at the cathode, which indicates that deposition process is diffusion controlled.

4. CORROSION STUDY

4.1. Potentiodynamic Polarization Study

Electroplated specimens were subjected to corrosion study, and corrosion rates were determined by Tafel's extrapolation method. The corrosion data corresponding to coatings at different c.d. is given in Table 4. It may be noted that, the corrosion rate of coatings increase with c.d., may be due changed phase structure of the deposit. However, the corrosion rate was found to increase at very low c.d., may be due to tendency of the bath to transit from anomalous to normal codeposition [6]. The large variation in the Tafel's slope of cathodic polarization, shown in Table 4, indicates that protection efficacy of the coatings is cathode controlled. A comparison of polarization behaviors of mild steel with, and without Zn–Fe coating (at optimal condition) is shown in Fig. 2. It may also be noted that E_{corr} value of electroplated Zn–Fe coating is more negative than mild steel, evidencing the sacrificial protection of the coatings. In Fig. 2, it may be observed that at high positive potential, the anodic curve of coated specimen is same as mild steel, indicating that at higher potentials, the protection efficacy of the coating is lost. Based on the corrosion data, the deposit at 3.0 A/dm^2 with ~3.62 wt %Fe showed least corrosion rate (2.26×10^{-2} mmy^{-1}) compare to uncoated steel (18.64×10^{-2} mmy^{-1}), shown in Table 4.

Table 4. Corrosion parameters of Zn–Fe alloy coatings at different c.d. in potential ramp of –0.25 V to +1.0V from OCP at scan rate of 1 mV/s in 5% NaCl

Current density, A/dm^2	i_{corr}, μA cm^{-2}	E_{corr}/V, vs. Ag/AgCl	βc, mV/dec	βa, mV/dec	Corrosion rate ×10^{-2}, mm y^{1-}
1.0	12.26	–1.259	41.07	20.49	12.20
2.0	6.063	–1.240	54.63	37.85	8.82
3.0	1.556	–1.233	22.75	16.65	2.26
4.0	3.972	–1.233	29.31	20.12	5.78
5.0	8.023	–1.259	145.45	50.33	11.68
Mild steel	12.55	–0.774	245.51	64.47	18.64

4.2. Electrochemical Impedance Study

Electrochemical impedance spectroscopy, generally known as EIS technique is one of the powerful tools for studying the electrochemical behavior of the materials. In this technique, impedance behavior is being studied by the application of an AC signal (sinusoidal wave) [15]. The form of the current–voltage relationship of the impedance in an electrochemical system can also be expressed as

$$Z(\omega) = V(t)/I(t),$$

where $V(t)$ and $I(t)$ are the measurements of voltage and current in an AC system.

Generally, the impedance spectrum of an electrochemical system can be presented in Nyquist and Bode plots, which are representations of the impedance as a function of frequency. A Nyquist plot is displayed for the experimental data set $Z(Z_{re,i}, Z_{im,i}, \omega_i)$, ($i = 1, 2, ..., n$) of n points measured at different frequencies, with each point representing the real and imaginary parts of the impedance ($Z_{re,i}$, $Z_{im,i}$) at a particular frequency ω_i. A Bode plot is an alternative representation of the impedance. In a plot of phase angle, θ vs. logω, describing the frequency dependencies of the phase angle. Both plots usually start at a high frequency and end at a low frequency, which enables the initial resistor to be found more quickly.

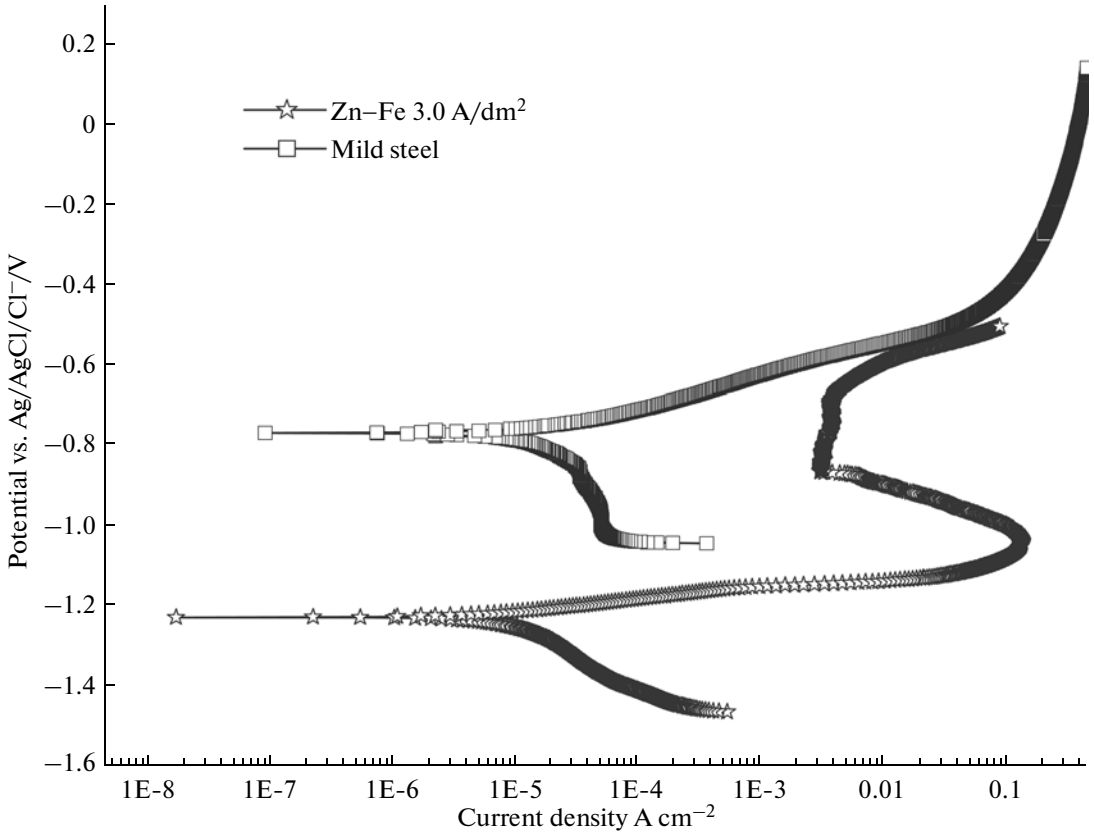

Fig. 2. Comparison of Tafel's behavior of mild steel with and without Zn–Fe alloy coating at scan rate of 1 mV/sec in 5% NaCl.

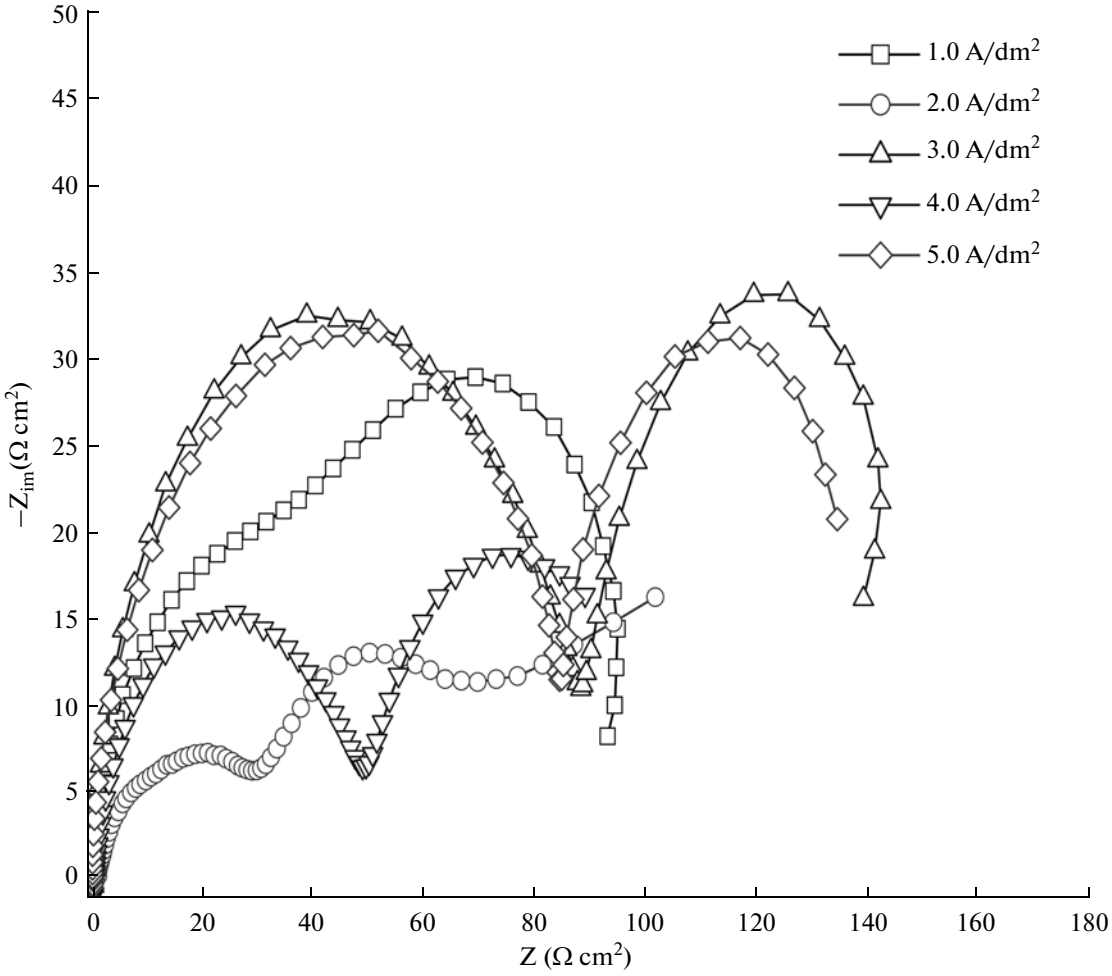

Fig. 3. Electrochemical impedance signals of electrodeposited Zn–Fe coatings developed at different current densities, in the frequency range of 20 mHz—100 kHz.

The Nyquist data points recorded for electroplated Zn–Fe alloys at different c.d.'s are shown in Fig. 3. The first capacitive loop is assigned to the charge transfer reaction R_{ct}. The second capacitive loop is assigned to the diffusion limited cathodic reduction of oxygen. The impedance response, is more stable in the case of optimal c.d. than at other c.d.'s. The impedance was found to decrease in relation with the breakdown of the air formed oxide layer, and then again increased slowly with the formation of corrosion products. From the results of Fig. 3, it is clear that in the initial stage of corrosion, a porous layer grew on the surface and accordingly zinc dissolution occurred through this porous oxide layer with oxygen reduction proceeding at the solution/oxide interface under diffusion control.

5. CYCLIC POLARIZATION STUDY

The cyclic polarization study, shown in Fig. 4 confirmed the formation of both air formed oxide layer, and corrosion product layer. The current density of backward scanning was higher than that of the forward scanning in the potential range of –0.3 V to –0.7 V, in relation to the breakdown of the air formed oxide layer, and it was lower than that of forward scanning in the potential range from –0.7 V to –1.0 V, due to the formation of corrosion products. This supported the fact that corrosion is initiated by pitting.

6. SEM ANALYSIS

SEM analysis showed that c.d. plays a significant role on the structure and homogeneity of the deposit. Variation in the surface morphology with c.d. is shown in Fig. 5. The coating was found to be very thin at 2.0 A/dm^2 (Fig. 5a) and bright at optimal c.d. 3.0 A/dm^2 (Fig. 5b). But at high c.d. the deposit was found to be very rough and porous as shown in Fig. 5c. The wt % Fe in the deposit was confirmed by EDX analysis as shown in Fig. 6.

7. X–RAY DIFFRACTION ANALYSIS (XRD)

The phases of the electrodeposited Zn–Fe alloy are very complicated depending on the chemical compo-

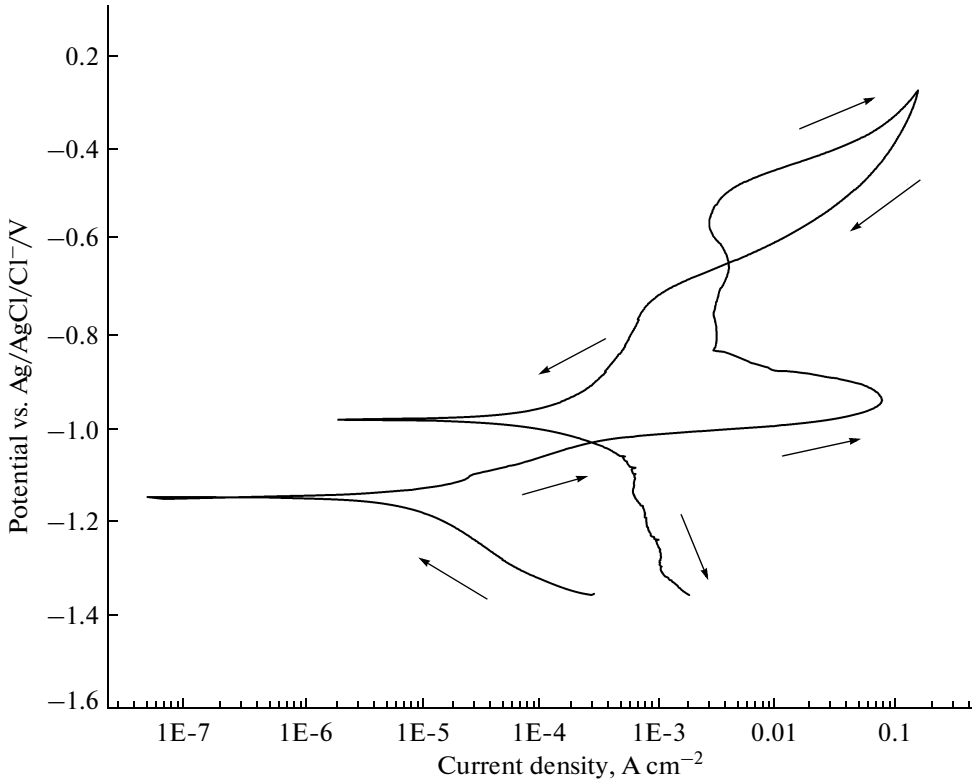

Fig. 4. Cyclic polarization curve of electrodeposited Zn–Fe alloy at 3.0 A/dm^2, at scan rate of 1 mV/sec in 5% NaCl.

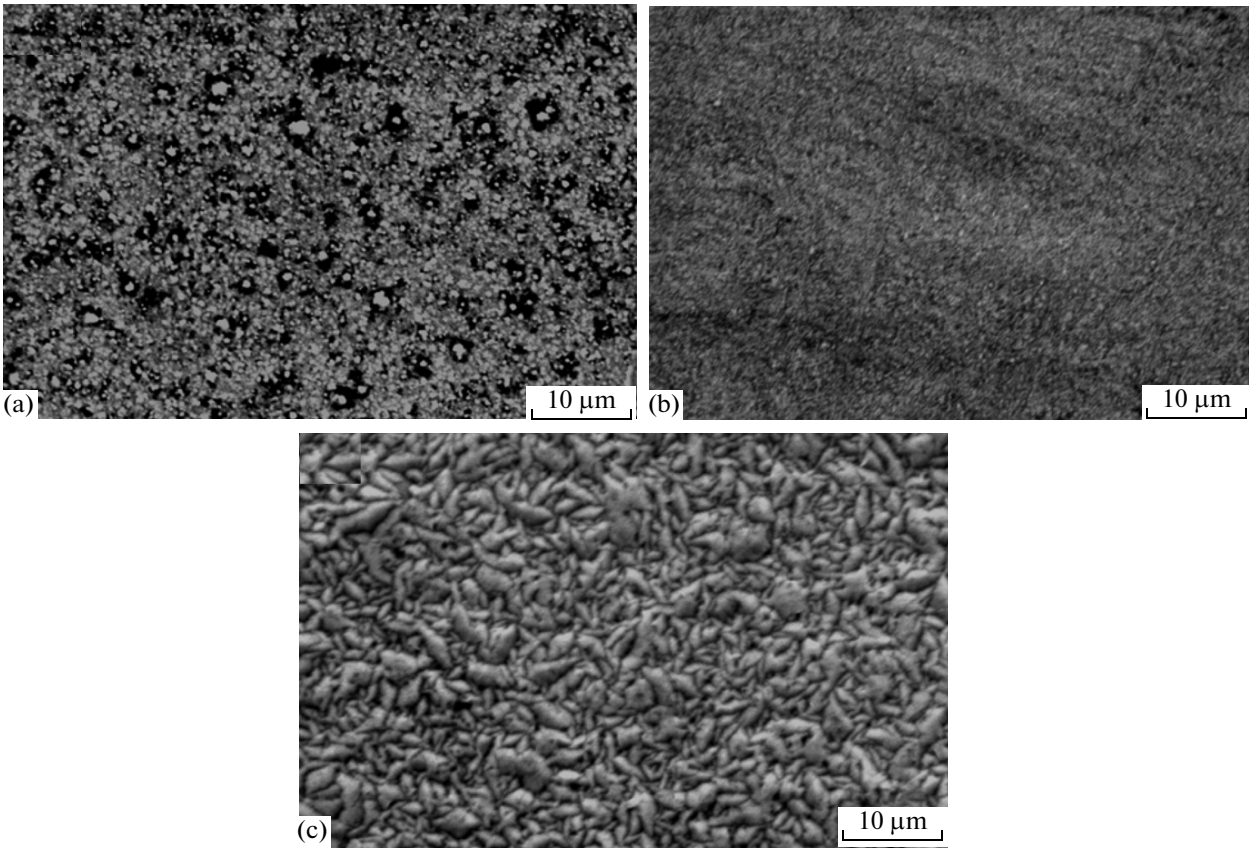

Fig. 5. Scanning electron microscopy (SEM) image of Zn–Fe alloys at 2.0 A/dm^2 (a), 3.0 A/dm^2 (b), and 5.0 A/dm^2 (c).

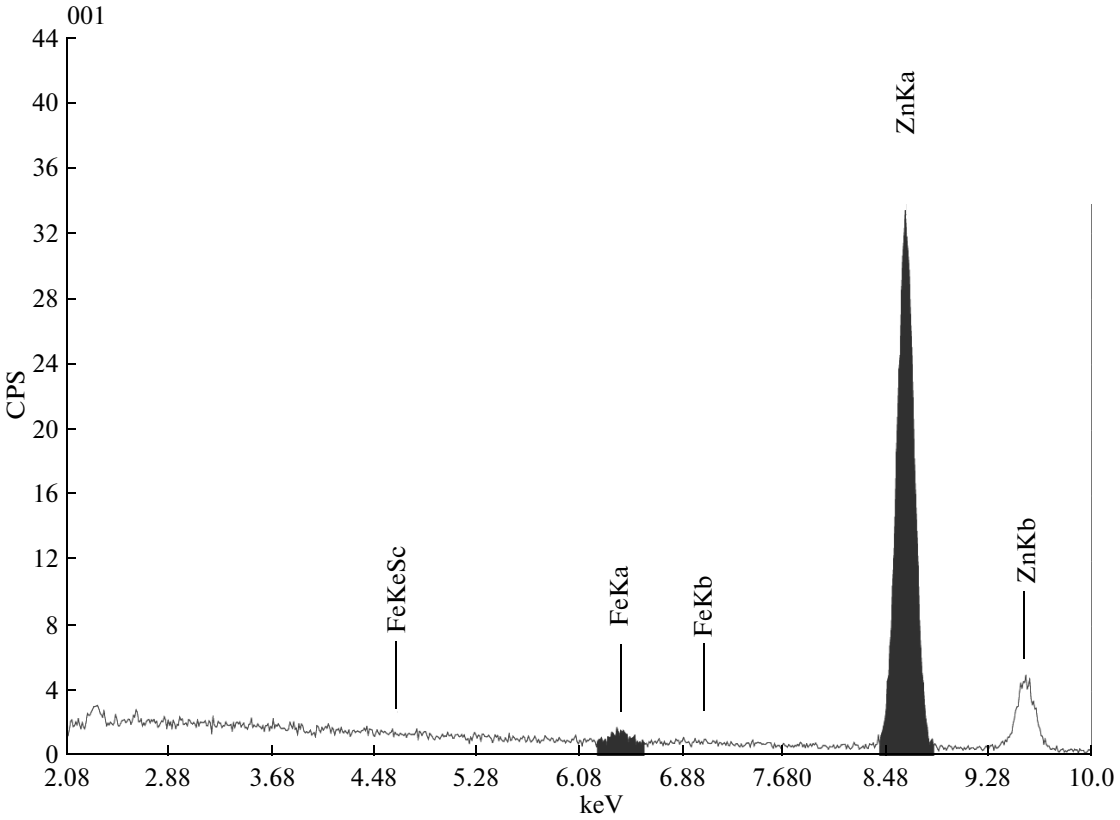

Fig. 6. EDX spectrum of Zn–Fe alloy deposit at optimum current density (3.0 A/dm^2), showing the wt.% Zn and Fe in the deposit.

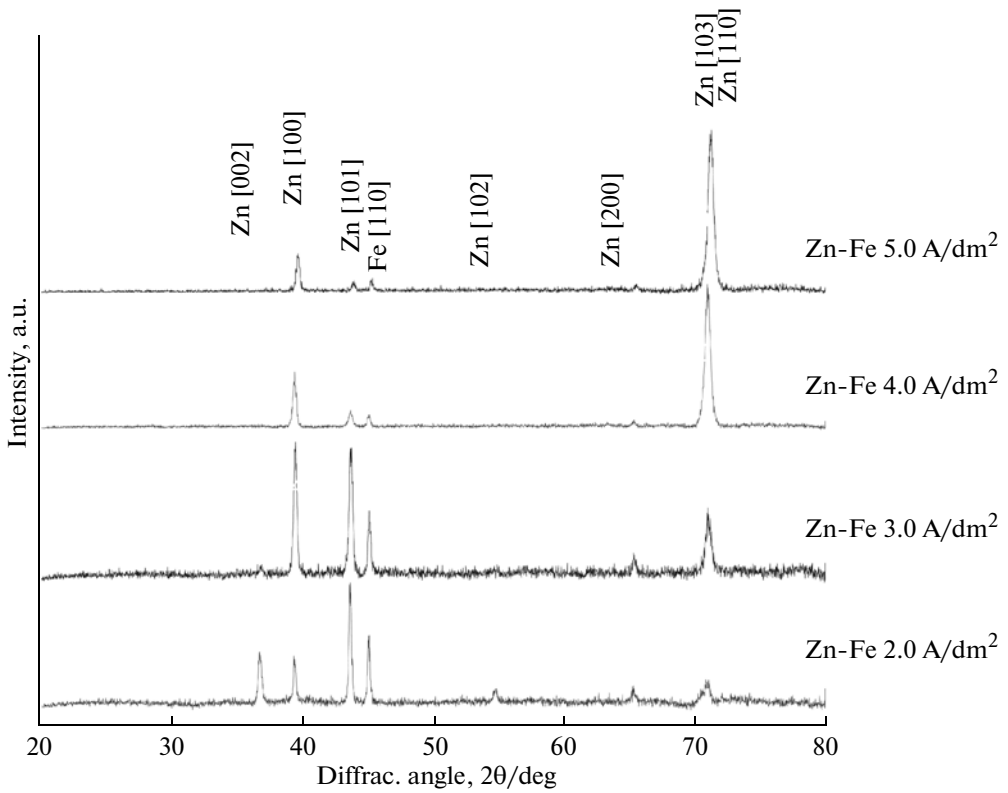

Fig. 7. X-ray diffraction profiles of electrodeposits obtained on mild steel from optimized bath at different current density, as mentioned on the plot.

sitions [16, 17]. XRD pattern of the Zn–Fe alloys, in Fig. 7 shows the formation of coatings having different phase structures; depending on the current density at which they are deposited. The XRD peaks reveals that Zn–Fe alloys with range composition have meta-stable structures, with many phases coexist. It may be noticed that, only relative intensities of the few phases of zinc (like (100), (101), (200) and (103) change among the deposited coatings, at different current densities, and hence different compositions [18]. It was found that the Zn–Fe alloy, at 3.0 A/dm^2 (with least corrosion rate) exhibits two intense peaks, corresponding to Zn with (100) and (101) phases.

8. CONCLUSIONS

1. A stable sulfate bath has bee proposed for electrodeposition of bright Zn–Fe alloy on to mild steel, using thiamine hydrochloride and citric acid as additives. The most suitable values of operating parameters and bath composition are presented in table. The optimum condition of for electrodeposition of Zn–Fe alloy are: cathode current density 3.0 A/dm^2, bath temperature 30°C, pH 4.0

2. The current density was found to play an important role on the production and properties of the deposit. No current density at which anomalous type of codepositon has changed to normal type.

3. Increase of Fe (less readily depositable metal) content in the deposit with temperature confirmed the diffusion controlled deposition process.

4. Shifting of E_{corr} value, (compared to that of bare substrate) towards anodic side indicated that the coatings offers sacrificial protection to the substrate.

5. At optimal composition and processing parameters, the Zn–Fe alloy showed minimum corrosion rate (2.26×10^{-2} mmy^{-1}).

6. EIS study showed two capacitive loops, one at high and other at low frequency ranges. The first capacitive loop was assigned to the charge transfer reaction and second capacitive loop was assigned to the diffusion limited cathodic reduction of oxygen.

7. The cyclic polarization study showed the improved corrosion resistance is due to barrier effect of oxide layer and corrosion products.

8. XRD study revealed that Zn–Fe alloy coatings, showing highest corrosion resistance is corresponding to Zn with (100) and (101) phases.

REFERENCES

1. Brenner, A., *Electrodeposition of Alloys: Principles and Practice*, N.Y.: Academic Press, 1963, vol. 2, p. 589.
2. Short, N.R., Abibsi, A., and Nennis, J.K., *Trans. Inst. Met. Fin.*, 1984, vol. 67, p. 73.
3. Abibsi, A., Dennis, J.K., and Short, N.R., *Trans. Inst. Met. Fin.*, 1991, vol. 69, p. 145.
4. Ramanauskas, R., Juskenas, R., Kalinicenko, L., and Garfias-Mesias, F., *J. Solid State Eletrochem.,* 2004, vol. 8, p. 416.
5. Narasimhamurthy, V. and Sheshadri, B.S., *Plating and Surface Finishing*, 1996, vol. 83, p. 75.
6. Nasser Kanani, *Electroplating-Basic Principles, Processes and Practice*, Berlin: Elsevier Pub. Ltd., 2006, p. 240.
7. Gomez, E. and Valles, E., *J. Electroanal. Chem.,* 1997, vol. 421, p. 157.
8. Jensen, J.D., Crichlow, G.W., and Gabe, D.R., *Trans. IMF.*, 1998, vol. 76, p. 187.
9. Zhang, Z., Leng, W.H., and Shao, H.B., et al., *J. Electroanal. Chem.*, 2001, vol. 517, p. 127.
10. Yang, C.Q., Long, Z.L., and Zhou, Y.C., *Trans. IMF.*, 2002, vol. 80, p. 161.
11. Diaz, S.L., Mattos, O.R., Barcia, O.E., and Fabri Miranda, F.J., *Electrochim. Acta.*, 2002., vol. 47, p. 4091.
12. Vogel, A.I., *Quantitative Inorganic Analysis, London: Longmans Green* Co, 1951, p. 245.
13. Trejo, G., et al., *J. Appl. Electrochem.*, 2003, vol. 33, p. 373.
14. Pardhasaradhy. *Practical Electroplating Hand Book*, Prentice Hall Incl. Pub., 1987, Chapter 3.
15. Yuan, X., Song, C., and Wang, H., et al. *Electrochemical Impedance Spectroscopy in PEM Fuel Cells—Fundamentals and Applications, London: Springer Publ.*, 2010, p. 248.
16. Lan, C.J., Liu, W.Y., Ke, S.T., and Chin, T.S., *Surface and Coat. Tech.*, 2006, vol. 201, p. 3103; *Fratesi R., Roventi G., Guliani G., J. Appl. Electrochem.*, 1997, vol. 27, p. 1088.
17. Fratesi, R., Roventi, G., and Guliani, G., J. Appl. electrochem., 1997, vol. 27, p. 1088.
18. Higashi, K., Fukushim, H., and Urakawa, T., *J. Electrochem. Soc.*, 1981, vol. 128, p. 2081.